Guided optical waves in planar heterostructures with negative dielectric constant

B. Prade, J. Y. Vinet, and A. Mysyrowicz*
Laboratoire d'Optique Appliquée, Ecole Polytechnique, Ecole Nationale Supérieure de Techniques Avancées, Centre de l'Yvette, 91 120 Palaiseau, France
(Received 1 May 1991; revised manuscript received 15 July 1991)

A detailed study of guided optical modes in planar heterostructures involving one or two media with negative dielectric constant is presented. The existence and the form of the solutions with respect to geometrical and physical parameters are derived. The cases of a metal between two dielectrics and a metal-dielectric-metal heterostructure are treated successively.

INTRODUCTION

Guided-optical-wave structures, consisting of a thin dielectric planar medium between two different dielectrics, are the subject of intense interest. They can accommodate propagating optical waves called guided modes,[1,2] which stay confined within the structure. As such, they play an important role in many optoelectronic applications. A well-known example is the diode laser, the operation of which relies crucially upon a built-in guided-mode structure.

An interesting situation occurs when a normal dielectric is surrounded by two media with negative dielectric constants. This is the case if metallic films are deposited on each side of a normal dielectric. It can also be the case for guided-wave structures consisting entirely of nonmetallic media, in certain limited frequency intervals. For instance, it is well known that semiconductors acquire a negative dielectric constant near resonances such as dipole-active phonons or excitons.

The symmetric situation may also occur, where a thin metallic film is embedded between normal dielectrics, or if a semiconductor with a negative dielectric constant in a certain energy interval is surrounded by normal dielectrics. Quantum-well structures may provide an example of the latter case.

The purpose of this paper is to derive all stable optical guided modes in an anomalous heterostructure, i.e., we look for the solutions of electromagnetic waves which are invariant along the propagation direction z. To the best of our knowledge, there is no complete study of all possible guided modes in such heterostructures. As already recognized by several authors for the case of symmetrical structures,[3–5] a special class of guided modes, called surface waves, can be sustained. These surface waves have field amplitudes with a maximum at the interface. In addition to surface waves, however, we will show that guided waves similar to those found in normal planar structures can also exist in certain cases. They have an oscillatory character inside the inner layer. We call them oscillating guided modes. The existence of the various stable solutions depends critically on the combination of the different indices and the sample geometry. In a lossless structure, these eigenmodes are characterized by a phase factor $\exp(ikn_{\text{eff}}z)$ involving a real parameter n_{eff} and the vacuum wave vector k. We restrict the discussion to the case of pure real dielectric constants: all media are considered to have no losses. This should provide a reasonable approximation in many cases. For example, in metals the imaginary part of the dielectric constant ϵ is small compared to the real negative part as long as $\omega<\omega_p$, where ω_p is the plasmon frequency. Specifically in Ag at room temperature $\mathrm{Re}(\epsilon)=-10$ and $\mathrm{Im}(\epsilon)=-0.37$ at wavelength $\lambda=510$ nm. By neglecting the imaginary part of ϵ, we can make use of the methods developed previously in classical guided-mode theory.[6,7] The central task is the determination of n_{eff}. n_{eff} depends both on the geometry of the structure through a parameter a (the inner layer thickness) and on physical parameters through the dielectric constants $\epsilon(\omega)$. Once $n_{\text{eff}}(\omega,a,\epsilon(\omega))$ is known, it is straightforward to derive the field components of the corresponding mode.

It is convenient to consider the problem in two successive steps. First we consider the dependence of n_{eff} on the geometry only (factor a), taking the wave frequency ω constant. We call this geometrical dispersion. Then, for fixed a, we study the dependence of n_{eff} with respect to frequency. Note that the frequency dependence $\epsilon(\omega)$ has to be included in the computation of the frequency dispersion $n_{\text{eff}}(\omega,a,\epsilon(\omega))$. We will restrict ourselves to the case of a plasma dispersion law, as relevant to metals. However, the case of a resonance in a semiconductor may be obtained without difficulty by introducing a Lorentz oscillator instead of the plasma dispersion law.

The paper is organized as follows. We first recall the features of surface waves at a planar interface in order to introduce the problem. We then treat the case of a negative dielectric constant (core) between two normal dielectric half spaces (cladding). Finally, we discuss the case of a dielectric core surrounded by a negative dielectric constant cladding.

I. SURFACE WAVES AT A PLANAR INTERFACE

In this section we derive the expression of n_{eff} in terms of the dielectric constants of the two media; we also express the form of the allowed modes and calculate the power flux carried by these modes. In order to fix the no-

tations, we consider a half space ($x>0$) having a positive dielectric constant $\epsilon_2=n_2^2$, and a second half space having a negative dielectric constant $\epsilon_1=-n_1^2$. Let us start by recalling Maxwell's equations:

$$\begin{aligned}&\text{curl } \mathcal{E}+\frac{\partial \mathcal{B}}{\partial t}=0\ ,\\ &\text{curl } \mathcal{H}-\frac{\partial \mathcal{D}}{\partial t}=0\ ,\\ &\mathcal{B}=\mu_0\mathcal{H}\ ,\\ &\mathcal{D}=\epsilon_0\epsilon\mathcal{E}=\epsilon_0 n^2\mathcal{E}\ .\end{aligned}\tag{1}$$

The time dependence of the monochromatic field is expressed as $\exp(-i\omega t)$. In order to simplify the notations let

$$\mathcal{E}=\mathbf{E}(x,y,z)e^{-i\omega t},\quad \mathcal{H}=\frac{1}{\mu_0 c}\mathbf{H}(x,y,z)e^{-i\omega t}\ .$$

The Maxwell equations reduce to

$$\text{curl } \mathbf{E}-ik\mathbf{H}=\mathbf{0},\quad \text{curl } \mathbf{H}+ikn^2\mathbf{E}=\mathbf{0}\ .\tag{2}$$

We are interested here in planar structures. Therefore the value of ϵ depends on only one coordinate normal to the interface. Without loss of generality we can direct the x axis along this normal, so that the form of the mode propagating in the z direction is

$$\mathbf{E}(x)e^{-i(\omega t-\beta z)},\quad \mathbf{H}(x)e^{-i(\omega t-\beta z)}\ \text{ with } \beta=kn_{\text{eff}}\ ,\tag{3}$$

the real quantity n_{eff} being called the effective index of the mode. Note that the field does not depend on y.

Combined with Maxwell's equations and the condition $\partial/\partial y=0$ this gives the relations

$$\begin{aligned}E_x&=\frac{in_{\text{eff}}\partial_x E_z}{k(n^2-n_{\text{eff}}^2)}\ ,\\ E_y&=\frac{-i\partial_x H_z}{k(n^2-n_{\text{eff}}^2)}\ ,\\ H_x&=\frac{in_{\text{eff}}\partial_x H_z}{k(n^2-n_{\text{eff}}^2)}\ ,\\ H_y&=\frac{in^2\partial_x E_z}{k(n^2-n_{\text{eff}}^2)}\ ,\end{aligned}\tag{4}$$

where E_z and H_z are solutions of the differential equations

$$[\partial_x^2+k^2(n^2-n_{\text{eff}}^2)]\begin{bmatrix}E_z\\ H_z\end{bmatrix}=0$$

$$\text{with } n=\begin{cases}n_2 & \text{for } x>0\\ in_1 & \text{for } x<0\ .\end{cases}\tag{5}$$

If we restrict the solutions to be evanescent in the two media and keep in mind the continuity requirement for components tangential to the interface, we obtain a transverse-magnetic (TM) solution only ($H_z=0$). This solution is

$$\begin{aligned}E_x&=A\frac{kn_{\text{eff}}}{u}e^{ux}\ ,\\ E_y&=0\ ,\\ E_z&=iAe^{ux}\ ,\\ H_x&=0\ ,\\ H_y&=-A\frac{kn_1^2}{u}e^{ux}\ ,\\ H_z&=0\ \text{ for } x<0\ ;\end{aligned}\tag{6}$$

$$\begin{aligned}E_x&=-A\frac{kn_{\text{eff}}}{w}e^{-wx}\ ,\\ E_y&=0\ ,\\ E_z&=iAe^{-wx}\ ,\\ H_x&=0\ ,\\ H_y&=-A\frac{kn_2^2}{w}e^{-wx}\ ,\\ H_z&=0\ \text{for } x>0;\end{aligned}\tag{7}$$

where A is a constant scaling factor and $u=k(n_{\text{eff}}^2+n_1^2)^{1/2}$, $w=k(n_{\text{eff}}^2-n_2^2)^{1/2}$, and

$$n_{\text{eff}}=\frac{n_1 n_2}{\sqrt{n_1^2-n_2^2}}\ ,\tag{8}$$

which shows that a mode exists only if $n_1\geq n_2$.

We see that the field is exponentially decreasing in the two media and hence strongly confined at the interface. For metals one recovers, in the limit $n_1=n_2$, the surface-plasmon mode resonance. For $n_1>n_2$, the propagating surface modes are in fact surface-plasmon-polariton modes which are a coherent superposition of surface plasmons and electromagnetic waves. The dispersion of such surface-plasmon polaritons is best visualized in a polariton diagram (see below).

The z component of the Poynting vector reads

$$S_z=\frac{\epsilon_0 c}{4}(\mathbf{E}\times\mathbf{H}^*+\mathbf{E}^*\times\mathbf{H})_z\ .\tag{9}$$

We find

$$S_z=\begin{cases}-|A|^2\dfrac{k^2 n_{\text{eff}} n_1^2}{u^2}e^{2ux} & \text{for } x<0\\ |A|^2\dfrac{k^2 n_{\text{eff}} n_2^2}{w^2}e^{-2wx} & \text{for } x>0\ .\end{cases}\tag{10}$$

In Fig. 1, we have plotted S_z as a function of the distance to the interface. Notice the opposite signs of S_z in the two media. Integration of S_z over the transverse direction yields the global power flux

$$P=\frac{k^2 n_{\text{eff}}}{2}\left[-\frac{n_1^2}{u^3}+\frac{n_2^2}{w^3}\right]|A|^2\ ,\tag{11}$$

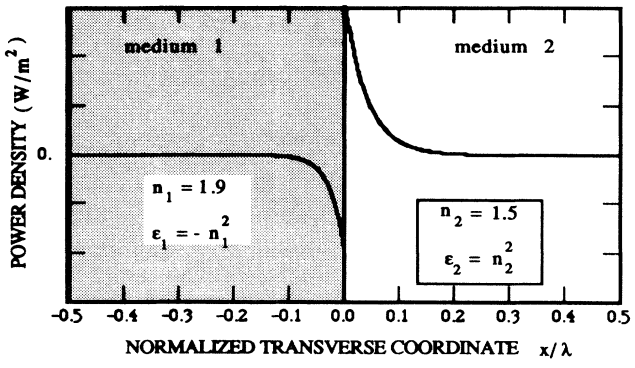

FIG. 1. Power flux density profile of a plasmon surface mode at an isolated interface. S_z is plotted in arbitrary units vs x, the distance from the interface, expressed in wavelength λ. Values of the refractive indices are shown in the figure. The curves are normalized such that the integrated power flux along x [Eq. (11)] equals 1 W/m.

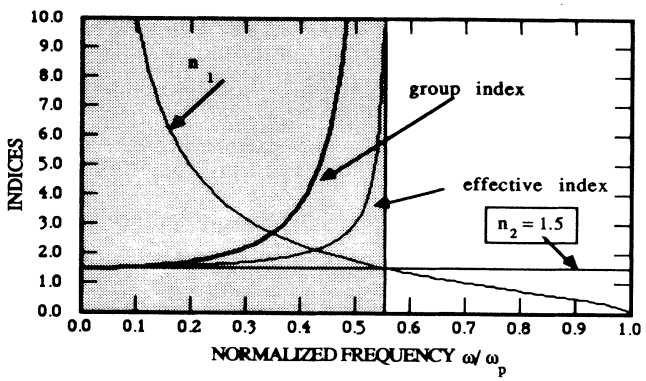

FIG. 2. Frequency dispersion of a plasmon surface mode at an interface between a normal dielectric and a medium with negative $\epsilon = -n_1^2$. The effective index and group index are plotted vs ω/ω_p for $n_2 = 1.5$.

which is always a positive quantity.

The above results are relevant for monochromatic waves, but physical waves are always a superposition of such waves for which the group velocity is the relevant concept. We are therefore led to study the dispersion. We see from Eq. (8) that the effective index does not depend explicitly on the light frequency. However, the dispersion of n_{eff} is contained in the variation of n_1 and n_2 with ω. Little dispersion arises from the normal dielectric ϵ_2, which is therefore taken as independent of frequency. In this paper, we will assume that the susceptibility of medium 1 is of the form

$$\epsilon(\omega) = 1 - \frac{\omega_p^2}{\omega^2} , \tag{12}$$

as is appropriate for lossless metals, with ω_p being the plasma frequency. The interesting region for our study is for $\epsilon_1 < 0$ and therefore $\omega < \omega_p$. We obtain

$$n_{\text{eff}} = n_2 \left[1 - \frac{n_2^2}{\omega_p^2/\omega^2 - 1} \right]^{-1/2} . \tag{13}$$

ω is thus restricted to the band $\omega < \omega_p/\sqrt{1+n_2^2}$. Instead of the group velocity, often the group index is used:

$$n_g = \frac{d(\omega n_{\text{eff}})}{d\omega} = \frac{n_2 \left[1 + \dfrac{n_2^2}{(\omega_p^2/\omega^2 - 1)^2} \right]}{\left[1 - \dfrac{n_2^2}{(\omega_p^2/\omega^2 - 1)} \right]^{-3/2}} . \tag{14}$$

In Fig. 2 we have plotted both the effective index and group index as a function of the reduced frequency ω/ω_p. The relation between the group velocity and the velocity of energy transfer may be expressed simply in the case of a quasimonochromatic wave.

In Maxwell's equations (1) we can substitute the quasimonochromatic field components

$$\begin{aligned} \mathcal{E} &= \int e^{-i(\omega t - \beta z)} \mathbf{E}(x,\omega) d\omega \\ &= e^{-i(\omega_0 t - \beta_0 z)} \int e^{-i\alpha(t-\beta' z)} \mathbf{E}(x, \omega_0 + \alpha) d\alpha , \\ \mu_0 c \mathcal{H} &= \int e^{-i(\omega t - \beta z)} \mathbf{H}(x,\omega) d\omega \\ &= e^{-i(\omega_0 t - \beta_0 z)} \int e^{-i\alpha(t-\beta' z)} \mathbf{H}(x, \omega_0 + \alpha) d\alpha , \end{aligned} \tag{15}$$

where ω_0 is the center of the band and β' is the derivative of β with respect to ω taken at point ω_0. This permits us to define the slowly varying part of the field

$$\mathbf{E}(t - \beta' z) = \int e^{-i\alpha(t-\beta' z)} \mathbf{E}(x, \omega_0 + \alpha) d\alpha . \tag{16}$$

By direct substitution in Maxwell's equations we obtain the following system of coupled partial derivatives equations:

$$\text{curl } \mathbf{E} - \beta_0 \mathbf{e}_z \times \mathbf{E} - i\beta' \mathbf{e}_z \times \frac{\partial \mathbf{E}}{\partial t} - i\frac{\omega_0}{c}\mathbf{H} + \frac{1}{c}\frac{\partial \mathbf{H}}{\partial t} = \mathbf{0} , \tag{17}$$

$$\begin{aligned} \text{curl } \mathbf{H} - \beta_0 \mathbf{e}_z \times \mathbf{H} - i\beta' \mathbf{e}_z \times \frac{\partial \mathbf{H}}{\partial t} + i\frac{\omega_0}{c}\mathbf{E} \\ - \frac{\partial(\epsilon\omega)}{\partial \omega}\frac{\partial \mathbf{H}}{\partial t} - i\mu_0 c \frac{\partial \epsilon}{\partial \omega}\frac{\partial^2 \mathbf{E}}{\partial t^2} = \mathbf{0} , \end{aligned} \tag{18}$$

where the time argument of the fields is $t' = t - \beta' z$. We shall neglect the last term of (18). By multiplying (17) by $\mathbf{H}^*$ and (18) by $\mathbf{E}^*$, then subtracting, integrating along the x direction, and finally identifying the real parts we find

$$\beta' = \frac{\dfrac{d}{dt}\displaystyle\int_{-\infty}^{\infty} \frac{d(\epsilon\omega)}{d\omega} |\mathbf{E}|^2 dx}{\dfrac{d}{dt}\displaystyle\int_{-\infty}^{\infty} S_z dx} . \tag{19}$$

We have supposed that the width of the frequency band is so narrow that the field distribution is the same for each component. This implies that we can separate the time dependence in both $|\mathbf{E}|^2$ and S_z so that the group velocity is expressed as

$$v_g = \frac{\int_{-\infty}^{\infty} S_z dx}{\int_{-\infty}^{\infty} \frac{d(\epsilon\omega)}{d\omega} |\mathbf{E}|^2 dx} . \tag{20}$$

The denominator is nothing but the energy density in a dispersive medium and consequently is always positive.[8] The sign of v_g is therefore the sign of the global power flux. We shall verify in the following sections that negative normalizing constants correspond to a negative group velocity.

We expect that in a planar guide geometry (involving two planar parallel interfaces) modes localized at both interfaces interact giving a richer set of solutions, which is the subject of the following two sections.

II. PLANAR SLAB CORE OF NEGATIVE DIELECTRIC CONSTANT

Consider a slab core of width $2a$ with negative dielectric constant $\epsilon_1 = -n_1^2$ surrounded by two claddings of dielectric constants $\epsilon_2 = n_2^2$ and $\epsilon_3 = n_3^2$ (see Fig. 3). In what follows, without loss of generality, we shall assume $n_3 < n_2$, the ratio value n_2/n_1 determining various types of solutions, which will be discussed in the present section. We first treat the general case of an asymmetric guide, then we give particular results for the symmetrical case. We examine the properties of the solutions, i.e., the effective index value and mode shape as a function of guide width $2a$ for fixed light frequency (geometric dispersion). Finally, we treat the dispersion problem giving the effective index variations as a function of frequency for fixed geometrical parameters.

We start by deriving n_{eff}, then we examine the analytic form of the corresponding field components.

A. Dispersion as a function of guide thickness

We first consider the general case of an asymmetric guide. By writing Eqs. (4) and (5) for each medium and continuity conditions for the tangential field components E_z, H_z, E_y, H_y, at both interfaces ($x=0$ and $2a$), we obtain a general dispersion equation, which is easily split into the following two separate equations related to transverse-electric (TE) and transverse-magnetic modes, respectively. We will find, as before, that only TM modes can exist:

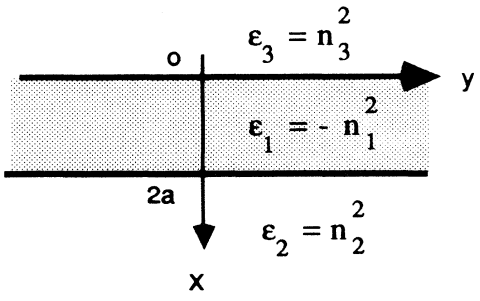

FIG. 3. Geometry and notations for the planar slab configuration. The inner layer is a medium with negative ϵ (such as a metal) and thickness $2a$.

$$\tanh(2U) = \begin{cases} -\dfrac{U(W_2+W_3)}{U^2+W_2W_3} & \text{(TE)} \\ \dfrac{n_1^2 U(n_3^2 W_2 + n_2^2 W_3)}{n_2^2 n_3^2 U^2 + n_1^4 W_2 W_3} & \text{(TM)} , \end{cases} \tag{21, 22}$$

where we have introduced the reduced real and positive transverse wave numbers

$$\begin{aligned} U &= ka\sqrt{n_1^2 + n_{\text{eff}}} , \\ W_2 &= ka\sqrt{n_{\text{eff}}^2 - n_2^2} , \\ W_3 &= ka\sqrt{n_{\text{eff}}^2 - n_3^2} , \end{aligned} \tag{23}$$

with U, W_2, and W_3 being positive, Eq. (21) can never be satisfied since the two members have opposite sign and therefore there is no TE-type solution. We now discuss the TM solutions given by Eq. (22). The components of the field are given as follows:

For $x \le 0$:

$$\begin{aligned} E_x &= \frac{n_{\text{eff}}}{n_3^2} H_y , \\ E_z &= A e^{W_3 x/a} , \\ H_y &= -ika A \frac{n_3^2}{W_3} e^{W_3 x/a} ; \end{aligned} \tag{24}$$

for $0 \le x \le 2a$:

$$\begin{aligned} E_x &= -\frac{n_{\text{eff}}}{n_1^2} H_y , \\ E_z &= A\left[\cosh(Ux/a) - \frac{Un_3^2}{W_3 n_1^2}\sinh(Ux/a)\right] , \\ H_y &= ika A \frac{n_1^2}{U}\left[\sinh(Ux/a) - \frac{Un_3^2}{W_3 n_1^2}\cosh(Ux/a)\right] ; \end{aligned} \tag{25}$$

for $x \ge 2a$:

$$\begin{aligned} E_x &= -\frac{n_{\text{eff}}}{n_2^2} H_y , \\ E_z &= A\left[\cosh(2U) - \frac{Un_3^2}{W_3 n_1^2}\sinh(2U)\right] e^{-W_2(x/a-2)} , \end{aligned} \tag{26}$$

$$H_y = ika A \frac{n_2^2}{W_2}\left[\cosh(2U) - \frac{Un_3^2}{W_3 n_1^2}\sinh(2U)\right] e^{-W_2(x/a-2)} .$$

By performing the Poynting vector integration on a cross section, we get the power flux

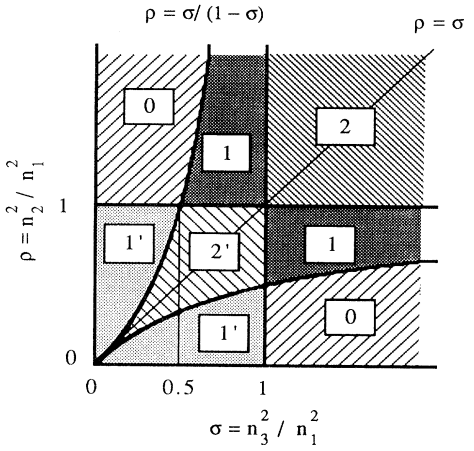

FIG. 4. Partition of the ρ,σ plane: the existence and number of solutions in the different regions are discussed in the text.

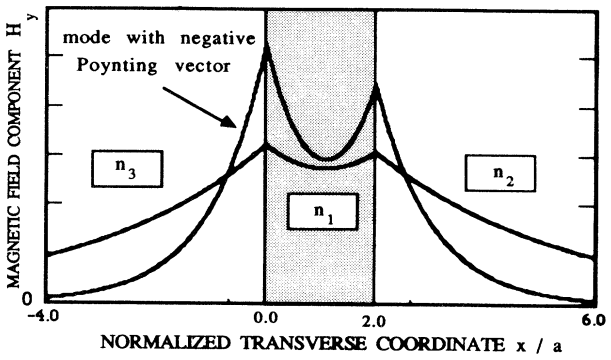

FIG. 6. Amplitude as a function of distance of the H_y component of the guided mode for region 2 of Fig. 4 in a planar slab structure in the direction x normal to the interfaces n_3/n_1 $(x/a=0)$ and n_1/n_2 $(x/a=2)$. Amplitudes are in arbitrary units. The following parameter values have been taken: $n_1=2(\epsilon_1=-4)$, $n_2=2.2$, $n_3=2.1$, $ka=0.15$.

$$P=\tfrac{1}{4}c\epsilon_0 k^2 a^3 A^2 \frac{n_1^4W_3^2-n_3^4U^2}{n_1^2W_3^2U^2}\left[2+\frac{n_1^2n_2^2}{W_2}\frac{V_2^2}{n_1^4W_2^4-n_3^4U^2}+\frac{n_1^2n_3^2}{W_3}\frac{V_3^2}{n_1^4W_3^2-n_3^4U^2}\right]. \tag{27}$$

We find that P can be negative, thus giving rise to a negative group velocity. The physical meaning of such negative solutions is not obvious, but we note that solutions with negative group velocity do not violate the principle of causality and that the energy density is always positive.[8] Negative group velocities are also encountered in semiconductors, for optical-phonon branches or near the top of conduction bands.

We now discuss the existence and properties of TM modes as a function of the optogeometrical parameters $2a$, n_1, n_2, and n_3 for fixed frequency.

A more convenient form of the implicit TM mode dispersion equation (22) is obtained by setting

$$V_2=ka\sqrt{n_1^2+n_2^2},\quad V_3=ka\sqrt{n_1^2+n_3^2} \tag{28}$$

(which gives $W_2^2=U^2-V_2^2$, $W_3^2=U^2-V_3^2$). Moreover, also let

$$X=\frac{U}{V_2},\quad R=\frac{V_3}{V_2},\quad \left[\frac{n_2}{n_1}\right]^2=\rho,\quad \left[\frac{n_3}{n_1}\right]^2=\sigma,\quad R^2=\frac{1+\sigma}{1+\rho}. \tag{29}$$

With these notations the dispersion equation becomes

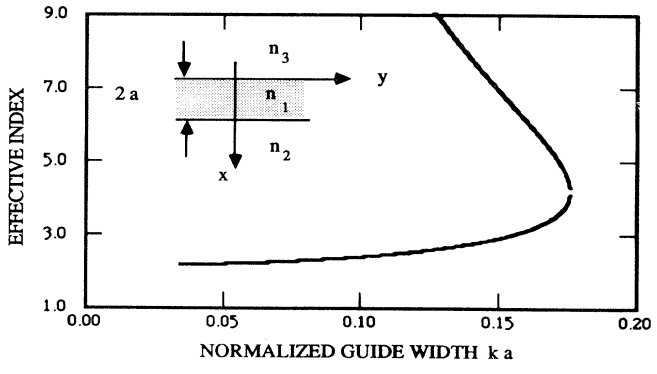

FIG. 5. Geometric dispersion of the effective index of surface modes in a planar slab structure with negative core index. This corresponds to region 2 of Fig. 4. The following values are adopted: $n_1=2$ $(\epsilon_1=-4)$, $n_2=2.2$, $n_3=2.1$ $(\rho=1.21$, $\sigma=1.10)$. Note the double-valued effective index for thickness $ka<0.18$. The upper branch corresponds to a mode with negative Poynting vector. The thickness is given in reduced units ka, where k is the vacuum wave vector.

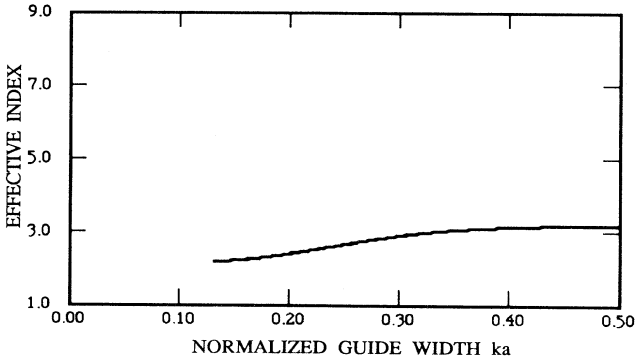

FIG. 7. Geometric dispersion of the effective index of a planar double heterostructure for region 1 of Fig. 4 as a function of inner layer thickness $2a$. The following indices have been taken: $n_1=2$ $(\epsilon_1=-4)$, $n_2=2.2$, $n_3=1.7$ $[\rho=1.21$, $\sigma=0.7225$, $\sigma/(1-\sigma)=2.6]$.

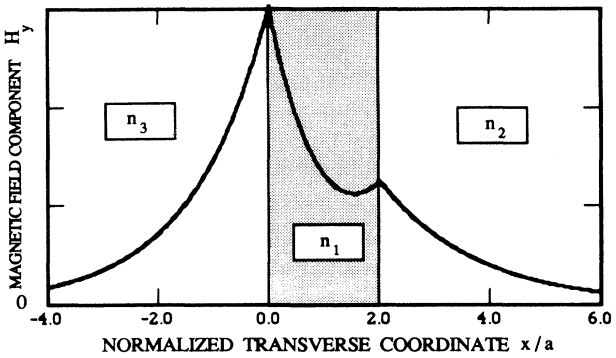

FIG. 8. H_y component of the surface mode in a double heterostructure for region 1 of Fig. 4 as a function of distance along x. The following parameters have been taken: $n_1=2$ ($\epsilon_1=-4$), $n_2=2.2$, $n_3=1.7$, $ka=0.3$.

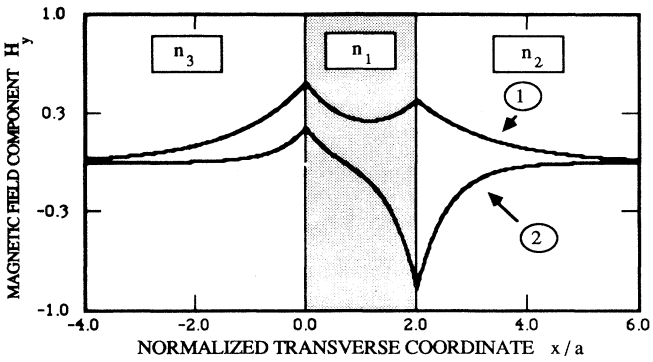

FIG. 10. H_y component of the surface mode in a double heterostructure for region 2′ of Fig. 4. The following values are adopted: $n_1=2$ ($\epsilon_1=-4$), $n_2=1.9$, $n_3=1.8$, $ka=0.3$. Curve 1 corresponds to the lower mode of Fig. 9.

$$\tanh(2V_2X)=\frac{X(\sigma\sqrt{X^2-1}+\rho\sqrt{X^2-R^2})}{\rho\sigma X^2+\sqrt{(X^2-1)(X^2-R^2)}}\ , \qquad (30)$$

with the restrictions $X>1$ and $R<1$.

Recall that solving the dispersion equation means determining n_{eff} as a function of V_2. Due to the implicit form of Eq. (30), it is more convenient to discuss the function $V_2(X)$, the determination of X from V_2, giving n_{eff}:

$$V_2=\frac{1}{4X}\ln\left[\frac{(1+A)(1+B)}{(1-A)(1-B)}\right]\ , \qquad (31)$$

with

$$A(X)=\frac{\sigma X}{\sqrt{X^2-R^2}},\quad B(X)=\frac{\rho X}{\sqrt{X^2-1}}\ .$$

It is clearly seen that the existence of solutions is restricted by the conditions $A,B>1$ or $A,B<1$.

By discussing these conditions we obtain a partition of the $(n_2/n_1, n_3/n_1)$ plane delimiting various domains with respect to number or cutoff properties of solutions. The discussion can be restricted to the $n_2>n_3$ area because the $n_2<n_3$ area may be obtained by symmetry. The case $n_2=n_3$ will be discussed separately in the context of symmetric structures. Figure 4 presents a summary of the discussion.

In region 0 satisfying the constraints $(\rho>1;\rho>\sigma/1-\sigma;\sigma<1)$ or $[n_2>n_1;n_3<n_1;n_2<n_1n_3/(n_1^2-n_3^2)^{1/2}]$, V_2 is never defined for any value of X and therefore no mode can exist. (While solutions involving a pure real effective index are strictly forbidden, nevertheless attenuated modes with complex n_{eff} do exist even if this system is assumed lossless. Such modes are called leaky waves. For large ka, such modes have vanishingly small attenuation, as seen from the fact that the single interface solution should be recovered in the limit of infinite thickness. They may be experimentally hard to distinguish from true surface modes in the presence of residual material losses.)

In region 2, when condition $\rho>\sigma>1$ ($n_2>n_3>n_1$) is achieved, the function $V_2(n_{\text{eff}})$ is continuous; it increases,

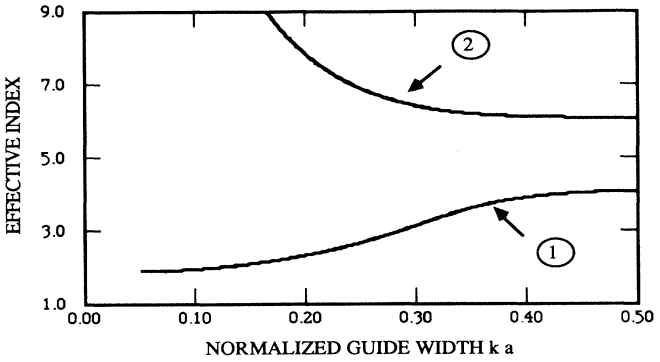

FIG. 9. Geometric dispersion of the effective index of a planar double heterostructure for region 2′ of Fig. 4. The following values are adopted: $n_1=2$ ($\epsilon_1=-4$) $n_2=1.9$, $n_3=1.8$ ($\rho=0.9025$, $\sigma=0.81$). The two modes would correspond to Fano modes in a symmetric case $n_2=n_3$.

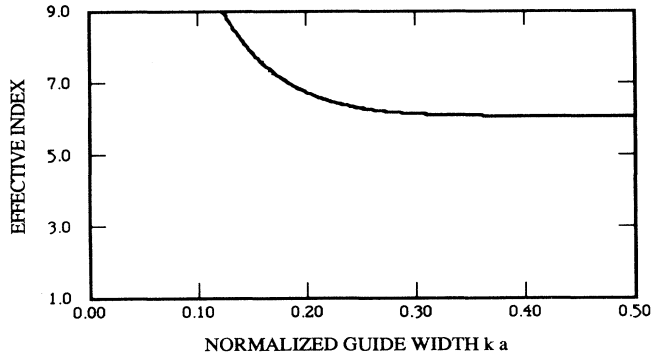

FIG. 11. Geometric dispersion of the effective index of a planar double heterostructure for region 1′ of Fig. 4. The following values are adopted: $n_1=2$ ($\epsilon_1=-4$), $n_2=1.9$, $n_3=1.3$ [$\rho=0.9025$, $\sigma=0.4225$, $\sigma/(1-\sigma)=0.7316$].

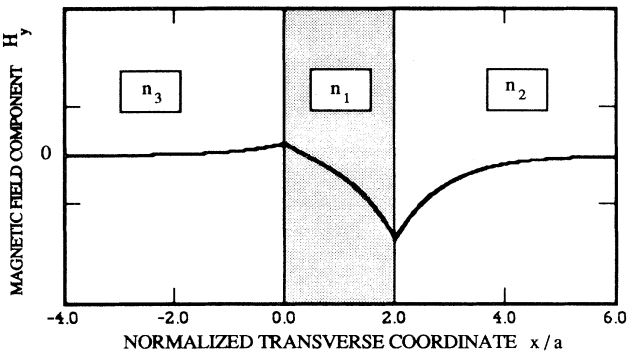

FIG. 12. Amplitude of the H_y component of the surface mode in a double heterostructure for region 1′ of Fig. 4 as a function of distance along x in arbitrary units. The following values are adopted: $n_1=2$, $n_2=1.9$, $n_3=1.3$, $ka=0.15$.

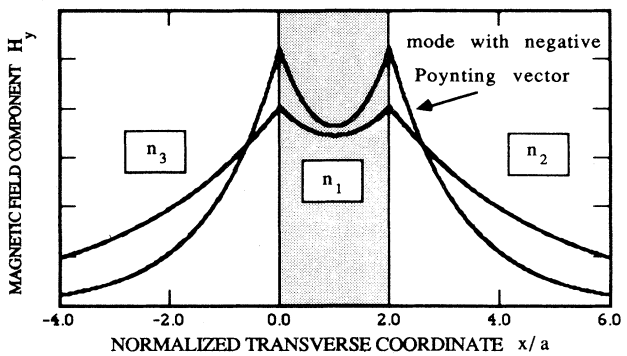

FIG. 14. Amplitude of the H_y field component of the surface mode for a symmetric slab (area $\rho>\sigma>1$ of Fig. 4). The following numerical parameters have been adopted: $n_1=2$ ($\epsilon_1=-4$), $n_2=2.2$, $ka=0.15$.

reaches a maximum, then decreases to zero. The dispersion curve $n_{\text{eff}}(ka)$ is thus doubled valued, admitting an upper branch having only a high cutoff. The lower branch has in addition a low cutoff at $W_2=0$. Let us emphasize that in this region $n_2>n_1$ and $n_3>n_1$ no solution exists for the isolated (n_1,n_2) or (n_1,n_3) interfaces. The coupling makes the existence of new modes possible, but only for small core thicknesses. For larger widths, the slab behaves like two isolated interfaces and no more solution can exist anywhere. The dispersion curve and the corresponding mode profile are plotted in Figs. 5 and 6, respectively.

In region 1 satisfying the constraints $(\rho>1;\rho<\sigma/1-\sigma;\sigma<1)$ or $[n_2<n_3;n_2>n_1n_3/(n_1^2-n_3^2)^{1/2}]$ only one solution with a lower cutoff can exist. One sees that for increasing values of ka, n_{eff} tends towards the value given by the isolated interface theory (see Figs. 7 and 8).

In region 2′ satisfying the constraints $(\rho>\sigma;\rho<\sigma/1-\sigma;\rho<1)$ two branches separated by a finite gap are seen to exist. The upper branch has no cutoff. The lower branch has a lower cutoff. In this region, for each interface, an isolated interface type solution would exist sepa-

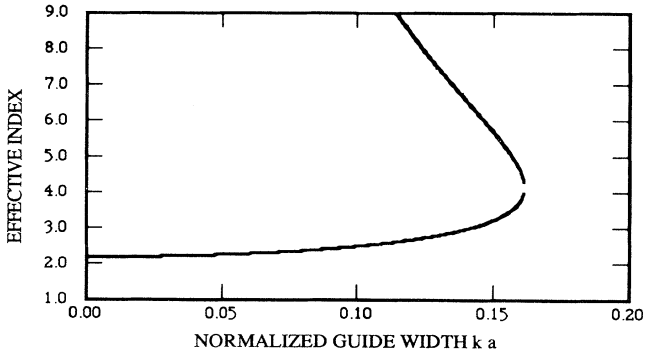

FIG. 13. Geometric dispersion of the effective index for a symmetric slab (area $\rho>\sigma>1$ of Fig. 4) as a function of inner layer thickness a expressed in reduced units. The following numerical parameters are adopted: $n_1=2$ ($\epsilon_1=-4$), $n_2=2.2$.

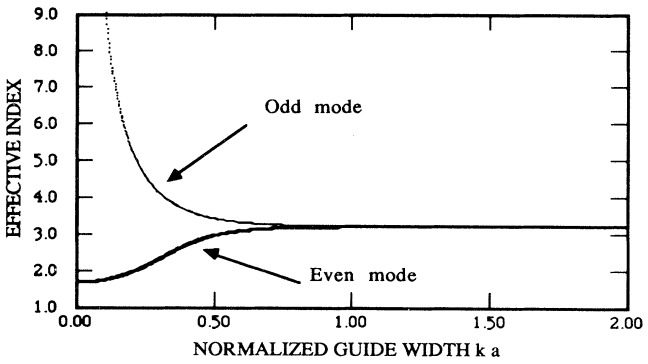

FIG. 15. Geometric dispersion of the effective index for a symmetric slab (area $\sigma<\rho<1$ of Fig. 4). Note the appearance of two distinct modes (Fano modes) for thicknesses $2a<1/k$, with k the incident light wave vector. The following numerical parameters have been adopted: $n_1=2$ ($\epsilon_1=-4$), $n_2=1.7$.

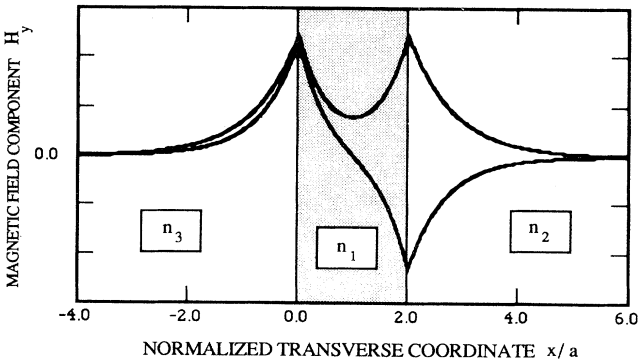

FIG. 16. Amplitude of the H_y field component for a symmetric slab (area $\sigma<\rho<1$ of Fig. 4). The following values have been adopted: $n_1=2$ ($\epsilon_1=-4$), $n_2=1.7$, $ka=0.5$ (for Au, the value of $2a$ is about 80 nm). Note the existence of the two Fano modes, also shown in Fig. 15.

TABLE I. Summary of the discussion for negative index core slab.

Area	Type of Solution
0	no solution
1	1 solution for $ka >$ cutoff
1′	1 solution for all ka
2	1 solution for cutoff $1 < ka <$ cutoff 2
	1 solution for $ka <$ cutoff 1, no solution for $ka >$ cutoff 2
2′	2 solutions for $ka >$ cutoff 1, otherwise no solution
diagonal $\rho > 1$	2 even solutions, similar to type 2
diagonal $\rho < 1$	similar to type 2′
	1 even mode with cutoff
	1 odd mode without cutoff
curve $\rho = \sigma/(1-\sigma)$	1 solution if $\sigma < 0.5$ with cutoff $X > \frac{1}{\sqrt{1-2\sigma}}$
	$\sigma > 0.5$ no solution
$\rho = \sigma = 1$	1 solution with cutoff
$\rho = 1, \sigma = \frac{1}{2}$	no solution

rately giving the two asymptotic values of n_{eff}. For small values of ka, these solutions becomes coupled, causing the observed dispersion (see Figs. 9 and 10). Such modes have been previously discussed under the names of Fano modes.[9]

In region 1′ satisfying the constraints $(\rho < 1; \rho > \sigma/1-\sigma)$ we obtain a unique solution without cutoff. Two isolated surface-type solutions may exist asymptotically, but only one is given by our analysis. As in case 0 there is a second solution having a complex n_{eff}, the imaginary part of which tends to zero as ka grows, giving asymptotically the isolated interface-type solution (see Figs. 11 and 12).

We now consider the special case of symmetric structures $(n_2 = n_3)$. For the sake of convenience, we choose the center of coordinates in the middle of the core. Due

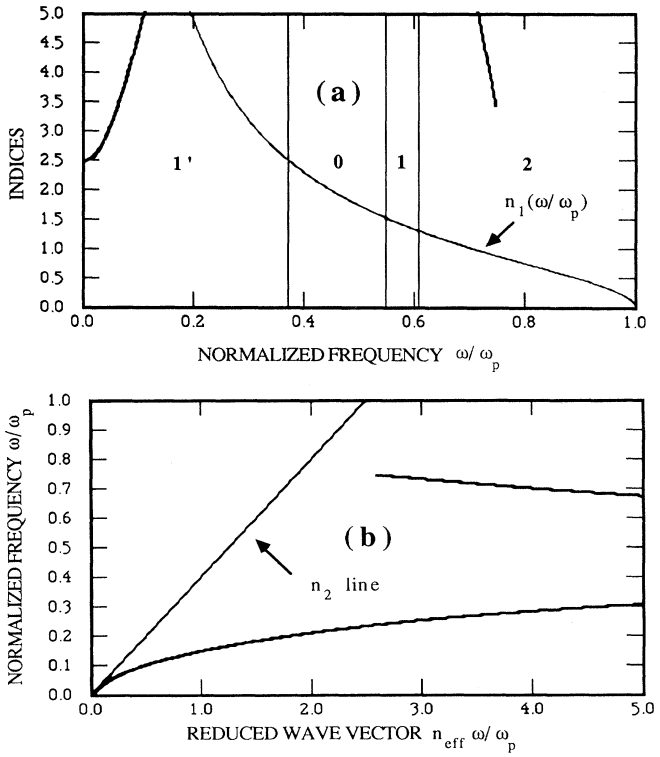

FIG. 17. (a) Frequency dispersion of the effective index n_{eff} (heavy line) and n_1 (light line) of the heterostructure shown in Fig. 3. Vertical bars delimit different regions of Fig. 4. The following values are adopted: $n_2 = 2.5$, $n_3 = 1.3$ $(\rho/\sigma > 2)$, $q = 0.1$. (b) Polariton dispersion curve of surface modes of a planar double heterostructure of inner layer thickness $2a$ (20 nm for gold) vs wave vector $\beta = kn_{\text{eff}}\omega/\omega_p$. $n_2 = 2.5$, $n_3 = 1.3$ $(\rho/\sigma > 2)$, $q = 0.1$. Note the negative slope of the upper curve corresponding to negative group velocity and the cutoff for $n_{\text{eff}}\omega/\omega_p < 2.8$. Also shown is the light dispersion in medium 2.

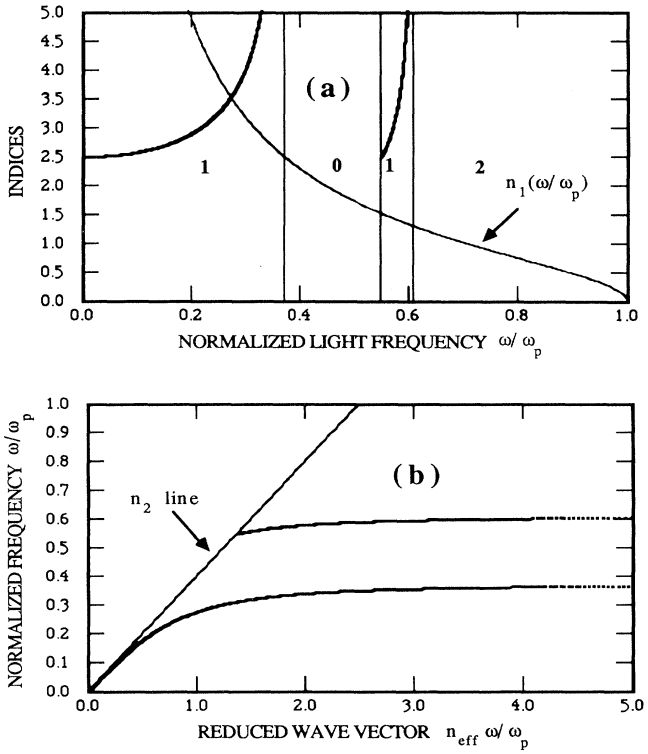

FIG. 18. (a) Same parameters as in Fig. 17(a), except $q = 2.0$. (b) Same parameters as in Fig. 17(b), except $q = 2.0$.

to the symmetric geometry the general dispersion equation can be split in two equations related to even and odd modes:

$$\tanh(U)=\begin{cases}\dfrac{n_1^2}{n_2^2}\dfrac{W}{U} & \text{(even solution)}\\ \dfrac{n_2^2}{n_1^2}\dfrac{U}{W} & \text{(odd solution);}\end{cases} \tag{32}$$

with

$$U=ka\sqrt{n_1^2+n_{\text{eff}}^2},\quad W=ka\sqrt{n_{\text{eff}}^2-n_2^2}\ ,\quad V=ka\sqrt{n_1^2+n_2^2}\ . \tag{33}$$

By defining the reduced variable $X=U/V>1$ and noting $\rho=(n_2/n_1)^2$, the dispersion equations become

$$\tanh(VX)=\begin{cases}\dfrac{\sqrt{X^2-1}}{\rho X} & \text{(even solution)} \quad (34)\\ \dfrac{\rho X}{\sqrt{X^2-1}} & \text{(odd solution)}\ . \quad (35)\end{cases}$$

It is clear that for $\rho<1$ both even and odd solutions can exist, and for $\rho>1$, only even solutions exist, since each member of Eq. (35) must be lower than unity. By inverting both equations, we finally can cast the dispersion relations under the following reverse but convenient form:

$$V=\begin{cases}\dfrac{1}{2X}\ln\left[\dfrac{\rho X+\sqrt{X^2-1}}{\rho X-\sqrt{X^2-1}}\right] & \text{(even solution)} \quad (36)\\ \dfrac{1}{2X}\ln\left[\dfrac{\sqrt{X^2-1}+\rho X}{\sqrt{X^2-1}-\rho X}\right] & \text{(odd solution)}\ . \quad (37)\end{cases}$$

In region $\rho>1$ ($n_2>n_1$), the even solutions are split into two branches (see Fig. 13); the corresponding shapes of the modes are plotted in Fig. 14. The upper branch corresponds to negative power solutions.

In region $\rho<1$ ($n_2<n_1$), we find one even solution and one odd solution, both without cutoff. This region is embedded in region 2′ of Fig. 4. It corresponds to the coupling between two identical plasmon modes which can be combined, giving odd and even supermodes. See Figs. 15 and 16. This whole discussion is summarized in Table I.

B. Dispersion as a function of light frequency

Having found the solutions of the stable modes at a fixed frequency as a function of geometry (geometrical dispersion), we now examine the frequency dependence of

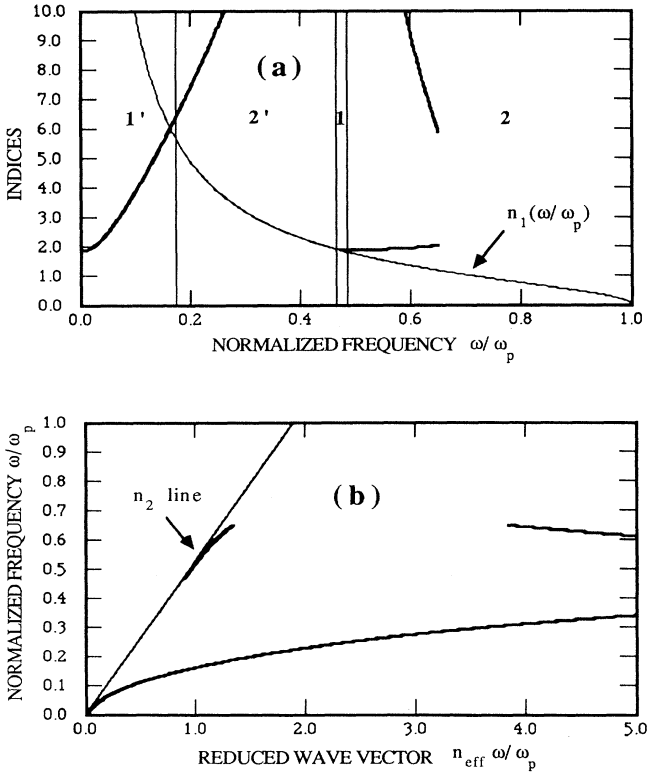

FIG. 19. (a) Effective index frequency dispersion. $n_2=1.9$, $n_3=1.8$ ($\rho/\sigma<2$), $q=0.1$. (b) Frequency dispersion. ω vs β. $n_2=1.9$, $n_3=1.8$ ($\rho/\sigma<2$), $q=0.1$.

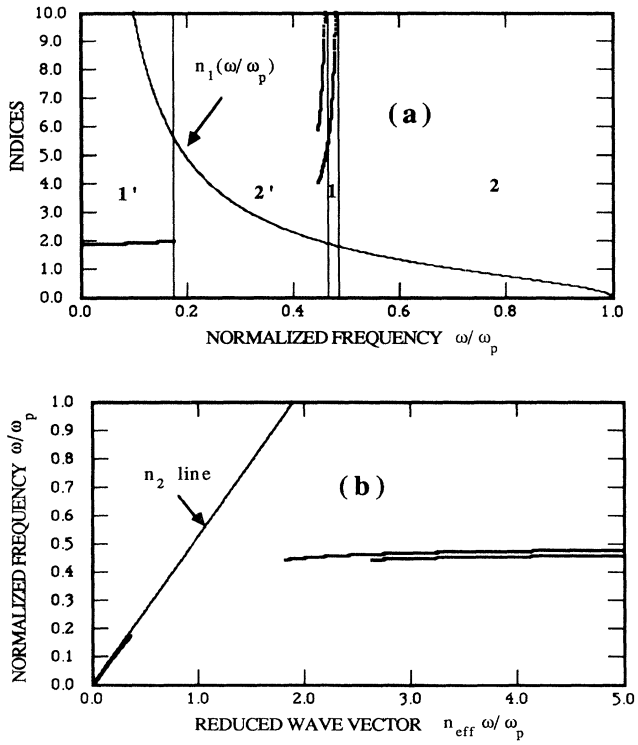

FIG. 20. (a) Effective index frequency dispersion. $n_2=1.9$, $n_3=1.8$ ($\rho/\sigma<2$), $q=2.0$. (b) Frequency dispersion. ω vs β. $n_2=1.9$, $n_3=1.8$ ($\rho/\sigma<2$), $q=2.0$. Note the cutoff.

the solution. As done previously, we shall make use of the plasma dispersion law given by Eq. (12).

By using the reduced frequency $\xi=\omega/\omega_p$ $(0<\xi<1)$ and the parameter $q=\omega_p a/c$, expressions (23) become

$$U=q\sqrt{1+(n_{\text{eff}}^2-1)\xi^2}\ ,$$
$$W_2=q\xi\sqrt{n_{\text{eff}}^2-n_2^2}\ , \tag{38}$$
$$W_3=q\xi\sqrt{n_{\text{eff}}^2-n_3^3}\ .$$

By substituting these explicitly frequency-dependent expressions in the general implicit dispersion equation (22), we get an implicit equation of the variable ξ, the solution of which gives the frequency dispersion.

By eliminating ξ between ρ and σ, we can see that the reduced frequency ξ may be represented by a straight line in the (ρ,σ) plane from the origin to infinity. Depending on the slope of the line, two scenarios may be encountered: (a) $(n_2/n_3)^2>2$: the path crosses areas 1′;0;1;2. (b) $(n_2/n_3)^2<2$: the path crosses the areas 1′;2′;1;2. In each case the effective index has been plotted with respect to the frequency parameter for various values of parameter q (see Figs. 17–20).

Often, the dispersion is presented in a frequency versus β ($\beta=kn_{\text{eff}}$) diagram (polariton diagram). This presentation has the advantage of showing the asymptotic limit for large n_{eff}. Such a polariton diagram is shown in Figs. 17(b), 18(b), 19(b), and 20(b).

III. PLANAR SLAB: CLADDING WITH NEGATIVE DIELECTRIC CONSTANT

Consider now the inverted structure, a planar slab core of ordinary dielectric constant ($\epsilon_1=n_1^2$ for $0<x<2a$) surrounded by two half space (claddings) of negative susceptibilities ($\epsilon_2=-n_2^2$ for $x>2a$, $\epsilon_3=-n_3^2$ for $0>x$). Again, we may assume $n_3<n_2$. The solutions of field equations found in Sec. II [Eqs. (24)–(26)] remain unchanged, but parameters W_2, W_3, V_2, and V_3 are now

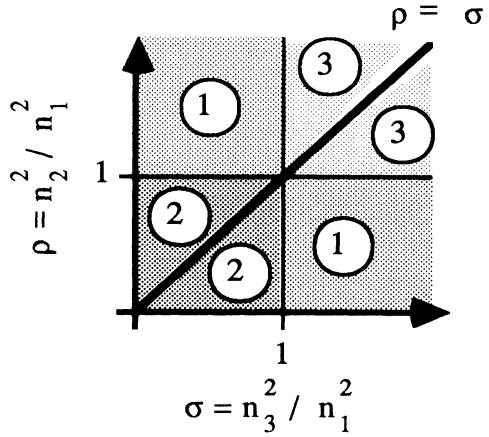

FIG. 21. Discussion of the existence of solutions for imaginary index claddings.

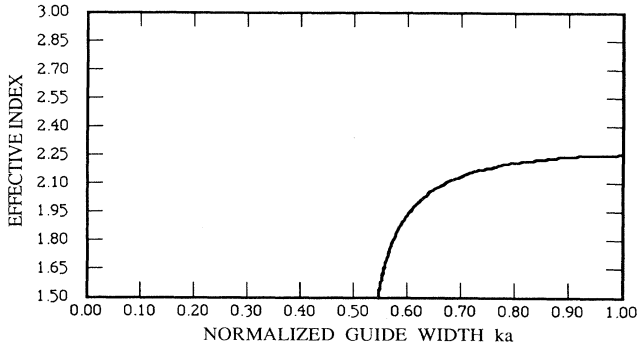

FIG. 22. Geometric dispersion curve of a normal dielectric core surrounded with media with negative ϵ, as a function of thickness expressed in reduced units ka. The following values are adopted: $n_1=1.5$, $n_2=2.0$ ($\epsilon_2=-4$), $n_3=1.3$ ($\epsilon_3=-1.69$), corresponding to area 1 of Fig. 21.

$$W_2=ka\sqrt{n_{\text{eff}}^2+n_2^2}\ ,\quad W_3=ka\sqrt{n_{\text{eff}}^2+n_3^2}\ ,$$
$$V_2=ka\sqrt{n_1^2+n_2^2}\ ,\quad V_3=ka\sqrt{n_1^2+n_3^2}\ . \tag{39}$$

The preceding definition of U [Eq. (23)] gives, for the ordinary index n_1,

$$U=ka\sqrt{n_{\text{eff}}^2-n_1^2}\ . \tag{40}$$

Recall that we look for solutions which are evanescent outside the core region of index n_1. Since U affects the type of solutions in the bounded core region only [see Eq. (40)], one must examine the case of either real or pure imaginary values, giving rise to evanescent ($n_1<n_{\text{eff}}$) or oscillating solutions ($n_{\text{eff}}<n_1$) in the core region.

Modes of the first family are TM modes, with a spatial dependence similar to those discussed in Sec. II [Eqs. (24)–(26)]; as before they correspond to surface modes. Modes of the second family, which may be divided into TE and TM modes, have features analogous to those of classical guided modes in ordinary dielectric structures. The two families will be treated in the following two subsections.

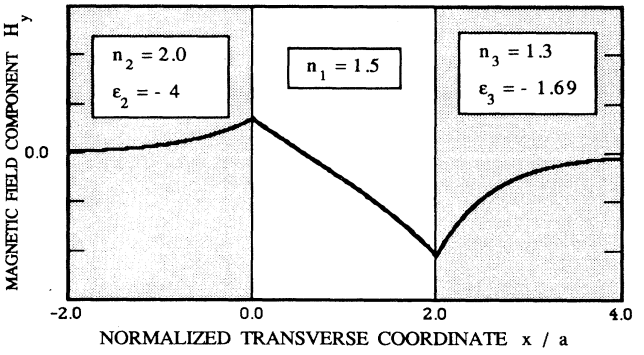

FIG. 23. Amplitude of the H_y field component of the surface mode of the heterostructure discussed in Fig. 2. $ka=0.6$.

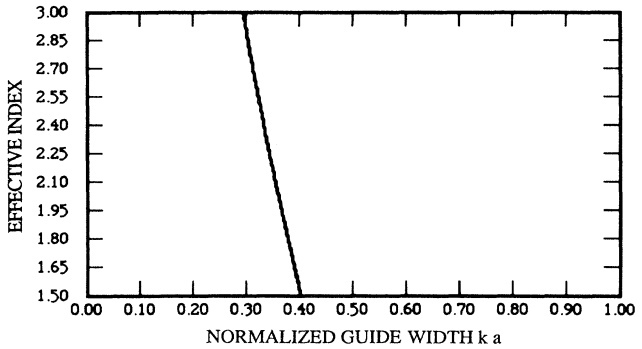

FIG. 24. Geometric dispersion curve for area 2 of Fig. 21. The following values are adopted: $n_1=1.5$, $n_2=1.4$ ($\epsilon_2=-1.96$), $n_3=1.3$ ($\epsilon_3=-1.69$).

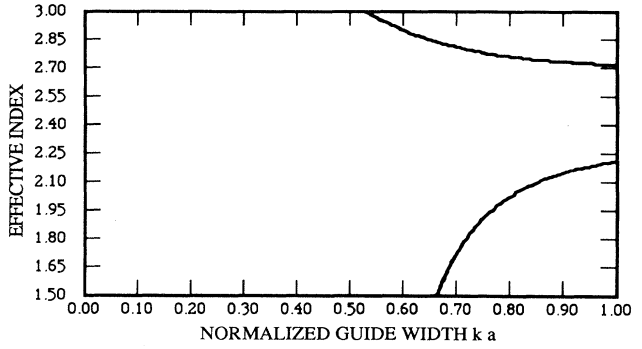

FIG. 26. Geometric dispersion curve for area 3 of Fig. 21. The following values are adopted: $n_1=1.5$, $n_2=2.0$ ($\epsilon_2=-4$), $n_3=1.8$ ($\epsilon_3=-3.24$).

A. Surface modes

1. Discussion of the existence of solutions

The TE and TM dispersion equations are now, with U real ($U=ka\sqrt{n_{\text{eff}}-n_1^2}$, $n_{\text{eff}}>n_1$),

$$\tanh(2U)=\begin{cases}-\dfrac{U(W_2+W_3)}{U^2+W_2W_3} & \text{(TE)} \quad (41)\\[2ex] \dfrac{n_1^2U(n_3^2W_2+n_2^2W_3)}{U^2n_2^2n_3^2+n_1^4W_2W_3} & \text{(TM)}\,, \quad (42)\end{cases}$$

which makes clear that, as in Sec. II, only TM modes can exist. In order to discuss the existence of the corresponding modes, it is convenient as before to introduce the parameters

$$X=\frac{U}{V_2},\quad R=\frac{V_3}{V_2},\quad \rho=\left[\frac{n_2}{n_1}\right]^2,\quad \sigma=\left[\frac{n_3}{n_1}\right]^2. \quad (43)$$

The assumption $n_3<n_2$ gives $\sigma<\rho$ and $R<1$; $X>0$. The dispersion equation reads

$$\tanh(2V_2X)=\frac{X(\sigma\sqrt{X^2+1}+\rho\sqrt{X^2+R^2})}{\rho\sigma X^2+\sqrt{X^2+1}\sqrt{X^2+R^2}}\,. \quad (44)$$

As in Sec. II, it is possible to give V_2 as a function of X:

$$V_2=\frac{1}{4X}\ln\left[\frac{(1+A)(1+B)}{(1-A)(1-B)}\right], \quad (45)$$

with

$$A(X)=\frac{\sigma X}{\sqrt{X^2+R^2}},\quad B(X)=\frac{\rho X}{\sqrt{X^2+1}}\,.$$

As usual, curve n_{eff} vs V_2 may be obtained by rotating the curve $V_2(n_{\text{eff}})$. Figure 21 summarizes this discussion.

Within the area 1 obeying the constraints $n_2>n_1$, $n_3<n_1$, we have one solution with a lower cutoff. That solution matches asymptotically the plasmon wave located at interface $x=2a$ (see Figs. 22 and 23).

Within area 2 ($n_3<n_2<n_1$), only one solution is seen

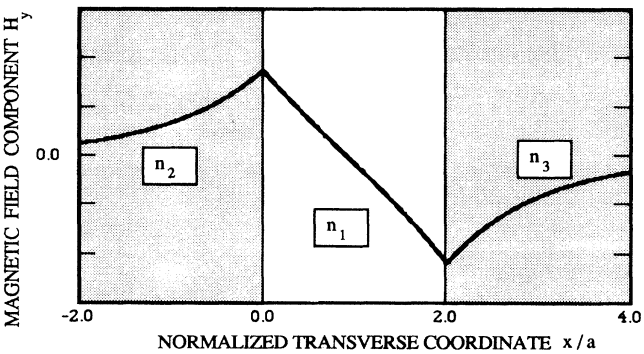

FIG. 25. Amplitude of the H_y field component of the surface mode shown in Fig. 24. This solution has a negative group velocity. The following values are adopted: $n_1=1.5$, $n_2=1.4$ ($\epsilon_2=-1.96$), $n_3=1.3$ ($\epsilon_3=-1.69$), $ka=0.3$.

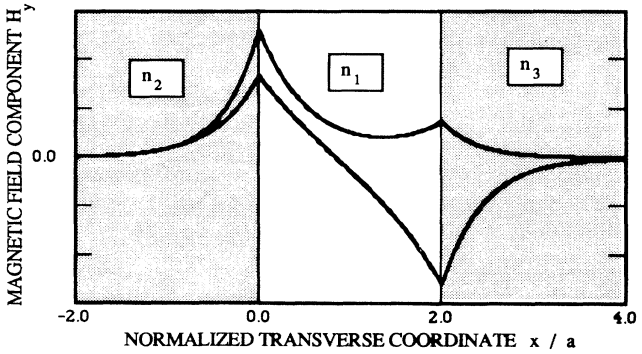

FIG. 27. Amplitude of the H_y field component for area 3 of Fig. 21. The following values are adopted: $n_1=1.5$, $n_2=2.0$ ($\epsilon_2=-4$), $n_3=1.8$ ($\epsilon_3=-3.24$), $ka=0.8$. The upper curve corresponds to the upper branch of Fig. 26.

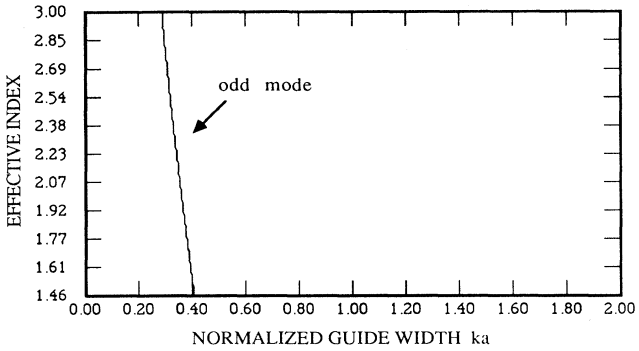

FIG. 28. Geometric dispersion curve for a symmetric slab. The following values are adopted: $n_1=1.457$, $n_2=1.3$ ($\epsilon_2=-1.69$).

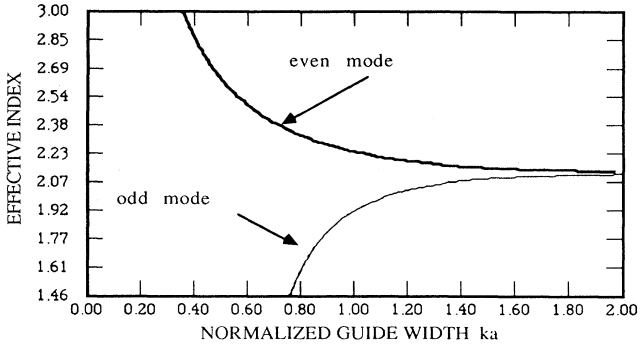

FIG. 29. Geometric dispersion curve for a symmetric slab. The following values are adopted: $n_1=1.457$, $n_2=2.0$ ($\epsilon_2=-4$).

to exist having an upper cutoff. The isolated interfaces cannot sustain any surface mode due to the plasmon existence condition (8), but the coupling between the interfaces allows the existence of this new mode. The corresponding dispersion curve and mode shape are plotted in Figs. 24 and 25.

Within area 3 ($n_2>n_3>n_1$), the solutions are split into two branches corresponding asymptotically to the plasmons located at each interface. The upper branch has no cutoff, the field intensity has no node in the core region and will involve even modes for the special case $n_2=n_3$. The lower branch has a lower cutoff, the corresponding fields have a node in the core region and will involve the odd modes of the symmetric structure (see Figs. 26 and 27).

The above analysis has to be completed by inspecting the properties of the symmetric slab. As in Sec. II, we adopt the more convenient notations

$$U=ka\sqrt{n_{\text{eff}}^2-n_1^2}\,,\quad W=ka\sqrt{n_{\text{eff}}^2+n_2^2}\,,$$
$$V=ka\sqrt{n_1^2+n_2^2}\,. \tag{46}$$

The general dispersion equation (42) splits up into the following two equations having even and odd solutions:

$$\tanh U=\begin{cases}\dfrac{n_1^2}{n_2^2}\dfrac{W}{U} & \text{(even TM solutions)}\\[2ex] \dfrac{n_2^2}{n_1^2}\dfrac{U}{W} & \text{(odd TM solutions)}\,.\end{cases} \tag{47}$$

As in Sec. II, let us set

$$X=\frac{U}{V},\quad \rho=\left[\frac{n_2^2}{n_1^2}\right]\,. \tag{48}$$

Within these notations we can rewrite Eqs. (47) under the form

$$V=\begin{cases}\dfrac{1}{2X}\ln\left[\dfrac{\rho X+\sqrt{X^2+1}}{\rho X-\sqrt{X^2-1}}\right] & \text{(TME)} \qquad (49)\\[2ex] \dfrac{1}{2X}\ln\left[\dfrac{\sqrt{X^2+1}+\rho X}{\sqrt{X^2+1}-\rho X}\right] & \text{(TMO)}\,. \qquad (50)\end{cases}$$

The discussion of the existence of solutions shows that (i) for $\rho<1$ ($n_2<n_1$) there is only one odd mode with a higher cutoff (see Fig. 28), (ii) for $\rho>1$ ($n_2>n_1$) there is one even mode without cutoff and one odd mode with a lower cutoff (see Fig. 29), (iii) for $\rho=1$ ($n_2=n_1$) only the odd mode can exist. Table II summarizes this discussion.

TABLE II. Summary of the discussion for negative index claddings.

Area	Type of solution
1	1 solution with a lower cutoff
2	1 solution with an upper cutoff
3	2 solutions one solution without cutoff one solution with a lower cutoff
diagonal $\rho>1$	one odd mode with an upper cutoff
diagonal $\rho<1$	2 solutions one even solution without cutoff one odd solution with a lower cutoff
$\rho=\sigma=1$	one odd mode

2. *Frequency dispersion*

Let us now discuss the existence and features of modes with respect to frequency. If the frequency is varied, the intrinsic dispersion laws of media 2 and 3 have to be taken into account.

By denoting ω_{2p} and ω_{3p} the plasma frequencies of media 2 and 3, respectively, we can express n_2 and n_3 as

$$n_2=\sqrt{\omega_{2p}^2/\omega^2-1},\quad n_3=\sqrt{\omega_{3p}^2/\omega^2-1}\ . \tag{51}$$

Without loss of generality, we shall assume $\omega_{3p}<\omega_{2p}$. By using reduced variables, we have

$$\tau=\frac{\omega_{3p}}{\omega_{2p}}\quad (0<\tau<1)\ ,\quad \xi=\frac{\omega}{\omega_{3p}}\quad (0<\xi<1)\ ,$$
$$q=\frac{\omega_{3p}a}{c}\ ; \tag{52}$$

$$n_2=\sqrt{1/\tau^2\xi^2-1},\quad n_3=\sqrt{1/\xi^2-1},\quad ka=q\xi\ ; \tag{53}$$

$$U=q\xi\sqrt{n_{\text{eff}}^2-n_1^2}\ ,\quad W_2=q\sqrt{(n_{\text{eff}}^2-1)\xi^2+1/\tau^2}\ ,$$
$$W_3=q\sqrt{(n_{\text{eff}}^2-1)\xi^2+1}\ . \tag{54}$$

When ξ is varied, the corresponding representative point in the ρ,σ plane describes a rectilinear path, which in general does not meet the origin. In Figs. 30 and 31 we have plotted the effective index versus reduced frequency ω/ω_{3p} for two typical values of parameters q and τ. In the same figures we have added the variations of n_2 and n_3. Note that there is a change of type of solution each time curves $n_2(\xi)$ or $n_3(\xi)$ cross the constant line n_1.

B. Oscillating guided modes

1. *Dispersion as a function of slab width*

Oscillating guided modes are obtained for values of n_{eff} lower than n_1. It is thus convenient to adopt the following new definition of U:

$$U=ka\sqrt{n_1^2-n_{\text{eff}}^2}\ . \tag{55}$$

The field components are now as follows.
For TE modes:

For $0\le x\le 2a$,

$$E_x=0\ ,$$
$$E_y=\frac{ika}{U}C\left[\sin(Ux/a)+\frac{U}{W_3}\cos(Ux/a)\right]\ , \tag{56}$$

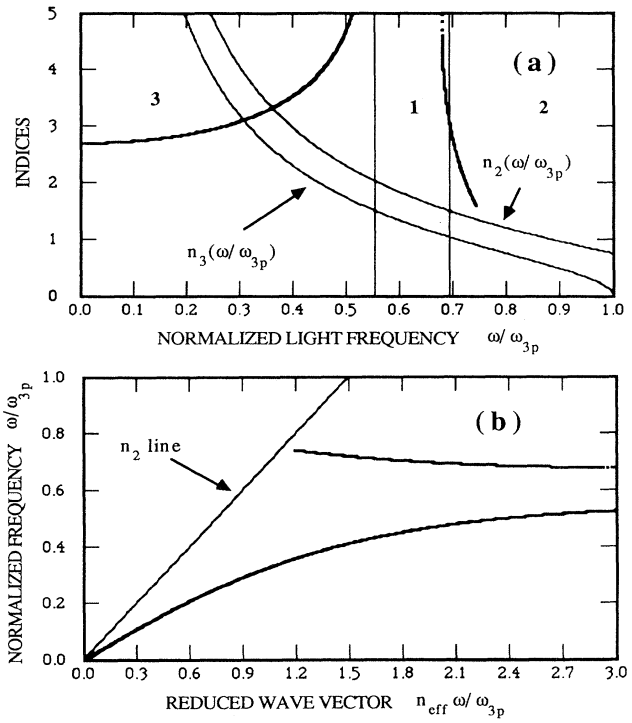

FIG. 30. (a) Effective index as a function of ω/ω_{3p}. ω_{3p} is the plasma frequency of medium 3. The following parameters have been chosen: $n_1=1.5$, $q=0.4$, $\tau=0.8$. (b) Frequency dispersion. ω vs $\beta=kn_{\text{eff}}\omega/\omega_{3p}$. The following parameters have been chosen: $n_1=1.5$, $q=0.4$, $\tau=0.8$.

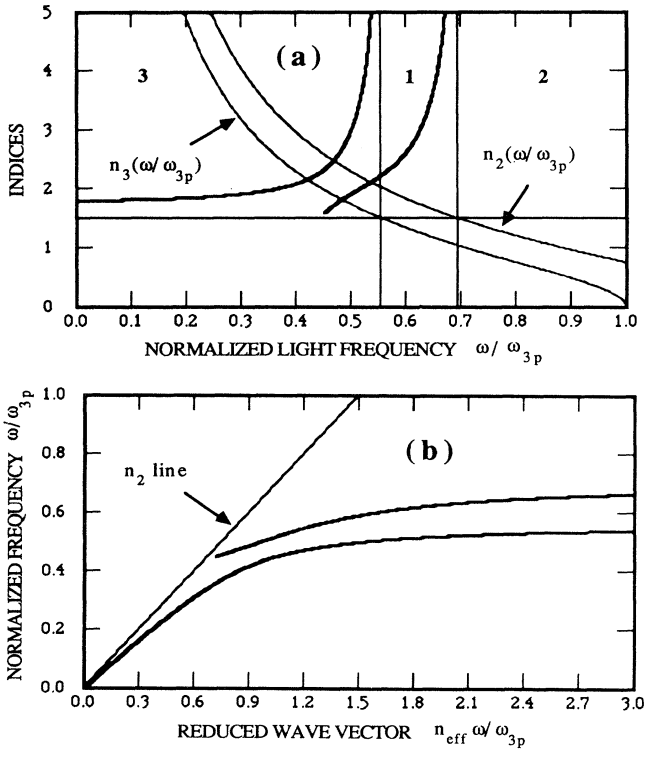

FIG. 31. (a) Frequency dispersion of the effective index as a function of the reduced frequency ω/ω_{3p}. The following values of the parameters have been adopted: $n_1=1.5$, $q=2$, $\tau=0.8$. (b) Frequency dispersion. ω vs $\beta=kn_{\text{eff}}\omega/\omega_{3p}$ for the following parameters: $n_1=1.5$, $q=2$, $\tau=0.8$.

$$E_z=0\ ,$$
$$H_x=-n_{\text{eff}}E_y\ ,$$
$$H_y=0\ , \tag{57}$$
$$H_z=C\left[\cos(Ux/a)-\frac{U}{W_3}\sin(Ux/a)\right]\ ;$$

for $x\le 0$,

$$E_x=0\ ,$$
$$E_y=ikaC\frac{e^{W_3x/a}}{W_3}\ , \tag{58}$$
$$E_z=0\ ,$$
$$H_x=-n_{\text{eff}}E_y\ ,$$
$$H_y=0\ , \tag{59}$$
$$H_z=Ce^{W_3x/a}\ ;$$

for $x\ge 2a$,

$$E_x=0\ ,$$
$$E_y=-i\frac{ka}{W_2}C\left[\cos(2U)-\frac{U}{W_3}\sin(2U)\right]e^{-W_2(x/a-2)}\ ,$$
$$E_z=0\ , \tag{60}$$
$$H_x=-n_{\text{eff}}E_y\ ,$$
$$H_y=0\ , \tag{61}$$
$$H_z=C\left[\cos(2U)-\frac{U}{W_3}\sin(2U)\right]e^{-W_2(x/a-2)}\ ;$$

For TM modes:

For $0\le x\le 2a$,

$$E_x=\frac{n_{\text{eff}}}{n_1^2}H_y\ ,$$
$$E_y=0\ , \tag{62}$$
$$E_z=A\left[\cos(Ux/a)-\frac{U}{W_3}\frac{n_3^2}{n_1^2}\sin(Ux/a)\right]\ ,$$
$$H_x=0\ ,$$
$$H_y=-i\frac{kan_1^2}{U}A\left[\sin(Ux/a)+\frac{U}{W_3}\frac{n_3^2}{n_1^2}\cos(Ux/a)\right]\ , \tag{63}$$
$$H_z=0\ ;$$

for $x\le 0$,

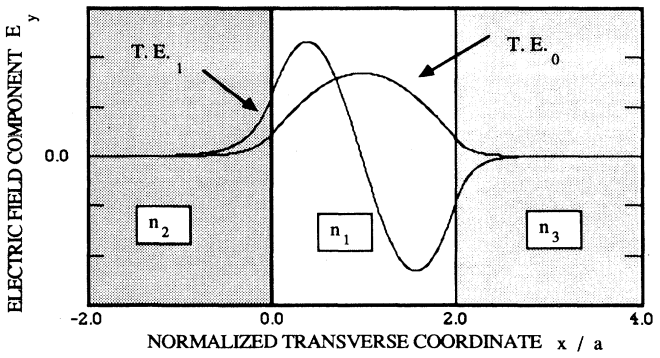

FIG. 33. Amplitude of the E_x component of TE_0 and TE_1 oscillating guided modes of Fig. 32. The following parameters have been assumed: $n_1=1.5$, $n_2=3$ ($\epsilon_2=-9$), $n_3=2$ ($\epsilon_3=-4$), $ka=2$. These parameters correspond to a layer of glass of thickness $2a=340$ nm surrounded with two metallic sheets of silver ($\epsilon_2=-9$) and gold ($\epsilon_3=-4$) for a wavelength 530 nm.

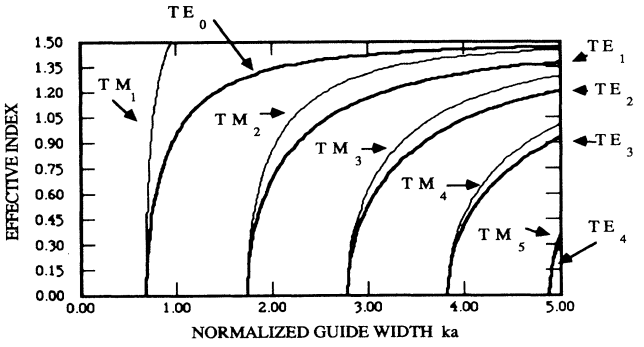

FIG. 32. Geometric dispersion curves for TE and TM oscillating guided modes. The following parameters are assumed: $n_1=1.5$, $n_2=3$ ($\epsilon_2=-9$), $n_3=2$ ($\epsilon_3=-4$).

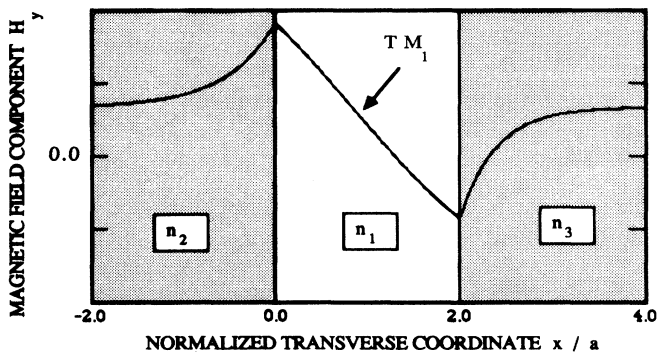

FIG. 34. Amplitude of the H_y component of TM_1 oscillating guided mode of Fig. 32. The following parameters have been assumed: $n_1=1.5$, $n_2=3$ ($\epsilon_2=-9$), $n_3=2$ ($\epsilon_3=-4$), $ka=0.8$.

$$E_x=\frac{n_{\text{eff}}}{n_3^2}H_y\ ,$$

$$E_y=0\ , \tag{64}$$

$$E_z=Ae^{W_3x/a}\ ;$$

$$H_x=0\ ,$$

$$H_y=-ika\frac{n_3^2}{W_3}Ae^{W_3x/a}\ , \tag{65}$$

$$H_z=0\ ;$$

for $x\geq 2a$,

$$E_x=\frac{n_{\text{eff}}}{n_2^2}H_y\ ,$$

$$E_y=0\ , \tag{66}$$

$$E_z=A\left[\cos(2U)-\frac{Un_3^2}{W_3n_1^2}\sin(2U)\right]e^{-W_2(x/a-2)}\ ;$$

$$H_x=0\ ,$$

$$H_y=ika\frac{n_2^2}{W_2}A\left[\cos(2U)-\frac{Un_3^2}{W_3n_1^2}\sin(2U)\right]e^{-W_2(x/a-2)}\ , \tag{67}$$

$$H_z=0\ .$$

The dispersion equations for TE and TM modes are, respectively,

$$\tan(2U)=\begin{cases}\dfrac{U(W_2+W_3)}{U^2-W_2W_3} & \text{(TE)} \quad (68)\\[2ex] -\dfrac{n_1^2U(n_3^2W_2+n_2^2W_3)}{U^2n_2^2n_3^2-n_1^4W_2W_3} & \text{(TM)}\ . \quad (69)\end{cases}$$

Note that the tan appears now, instead of tanh. We have a situation similar to the case of an ordinary heterostructure with positive dielectric constants. Modes will always exist above a critical thickness. Defining the variable $X=U/V_2$ and the parameter $R=V_3/V_2<1$, $[0<X<n_1/(n_1^2+n_2^2)^{1/2}$ with $V_2=ka(n_1^2+n_2^2)^{1/2}$ and $V_3=ka(n_1^2+n_3^2)^{1/2}]$ the inverted dispersion equations become

$$V_2=\begin{cases}\dfrac{1}{2X}\left[-\arctan\dfrac{X}{\sqrt{R^2-X^2}}-\arctan\dfrac{X}{\sqrt{1-X^2}}+k\pi\right] & \text{(TE)}\ , \quad (70)\\[2ex] \dfrac{1}{2X}\left[\arctan\dfrac{\sigma X}{\sqrt{R^2-X^2}}+\arctan\dfrac{\rho X}{\sqrt{1-X^2}}+k\pi\right] & \text{(TM)}\ , \quad (71)\end{cases}$$

which facilitates the discussion of the existence and cutoffs of the modes. We see that for ka tending towards infinity, there exists an infinity of modes obeying Eqs. (70) and (71), that we shall refer to as TE_{k+1} and TM_k modes, respectively. The situation is roughly analogous to that of guided modes in normal dielectric planar structures. The cutoff values are, however, different. One can see that TE_k and TM_{k+1} modes have a common cutoff given by

$$(ka)_{\text{inf}}=\frac{1}{2n_1}\left[-\arctan\frac{n_1}{n_3}-\arctan\frac{n_1}{n_2}+k\pi\right]\ . \tag{72}$$

Let us point out that the TM_1 mode has a specific behavior: it also has a higher cutoff given by

$$(ka)_{\text{sup}}=\frac{1}{2n_1^2}\left[\frac{n_3^2}{\sqrt{n_1^2+n_3^2}}+\frac{n_2^2}{\sqrt{n_1^2+n_2^2}}\right]\ . \tag{73}$$

The dispersion curves of the two families of modes have been plotted in Fig. 32. We have represented the spatial dependence of these modes in Figs. 33–35. Indexation of TE and TM modes has been determined in order to be consistent with the number of nodes of the field amplitudes.

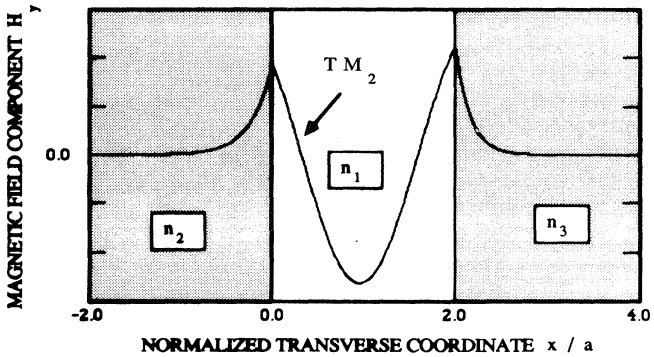

FIG. 35. Amplitude of the H_y component of TM_2 oscillating guided mode of Fig. 32. The following parameters have been adopted: $n_1=1.5$, $n_2=3$ ($\epsilon_2=-9$), $n_3=2$ ($\epsilon_3=-4$), $ka=2$.

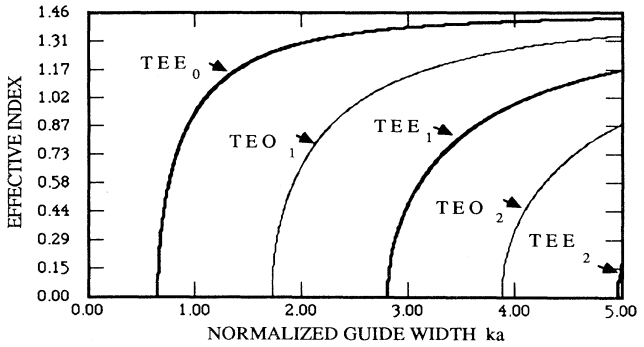

FIG. 36. Geometric dispersion of oscillating guided TE modes for a symmetric slab. The following parameters have been adopted: $n_1=1.457$, $n_2=2.0$ ($\epsilon_2=-4$).

2. *Symmetric case:* $n_2=n_3$

When $n_2=n_3$, we reduce the parameters and variables to the set

$$U=ka\sqrt{n_1^2-n_{\text{eff}}^2}\,,\quad W=ka\sqrt{n_{\text{eff}}^2+n_2^2}\,,\quad V=ka\sqrt{n_1^2+n_2^2}\,. \tag{74}$$

Then the dispersion equations are split into even and odd equations, giving four types of modes determined by

$$\tan U=\begin{cases}\dfrac{W}{U} & \text{(even TE solution)} \quad (75)\\[2ex] -\dfrac{U}{W} & \text{(odd TE solution)}\,, \quad (76)\end{cases}$$

$$\tan U=\begin{cases}-\dfrac{n_1^2}{n_2^2}\dfrac{W}{U} & \text{(even TM solution)} \quad (77)\\[2ex] \dfrac{n_2^2}{n_1^2}\dfrac{U}{W} & \text{(odd TM solution)}\,. \quad (78)\end{cases}$$

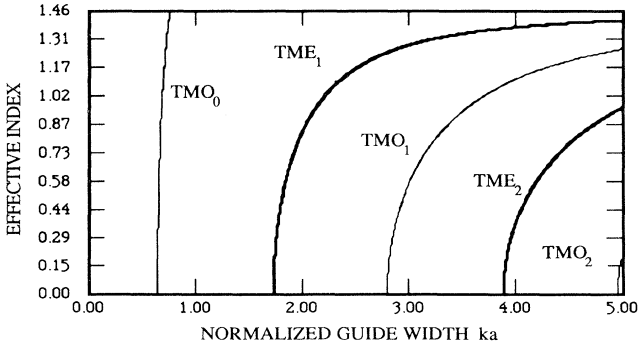

FIG. 37. Geometric dispersion of oscillating guided TM modes for a symmetric slab. The following parameters have been adopted: $n_1=1.457$, $n_2=2.0$ ($\epsilon_2=-4$).

An alternate useful form, which allows indexation of modes, is

$$V=\begin{cases}\dfrac{1}{X}\left[p\pi+\arctan\left(\sqrt{1/X^2-1}\right)\right] & \text{(TEE)} \quad (79)\\[2ex] \dfrac{1}{X}\left[p\pi-\arctan\left[\dfrac{X}{\sqrt{1-X^2}}\right]\right] & \text{(TEO)} \quad (80)\\[2ex] \dfrac{1}{X}\left[p\pi-\arctan\left[\dfrac{1}{\rho}\sqrt{1/X^2-1}\right]\right] & \text{(TME)} \quad (81)\\[2ex] \dfrac{1}{X}\left[p\pi+\arctan\left[\dfrac{\rho X}{\sqrt{1-X^2}}\right]\right] & \text{(TMO)}\,. \quad (82)\end{cases}$$

The geometric dispersion curves of these four families are shown in Figs. 36 (TE) and 37 (TM).

3. *Frequency dispersion*

When the frequency is varied, we can introduce, as in Sec. III A 2, parameters $\xi=\omega/\omega_{3p}$, $\tau=\omega_3/\omega_{2p}$, and $q=\omega_{3p}a/c$, and discuss the resulting dispersion as before.

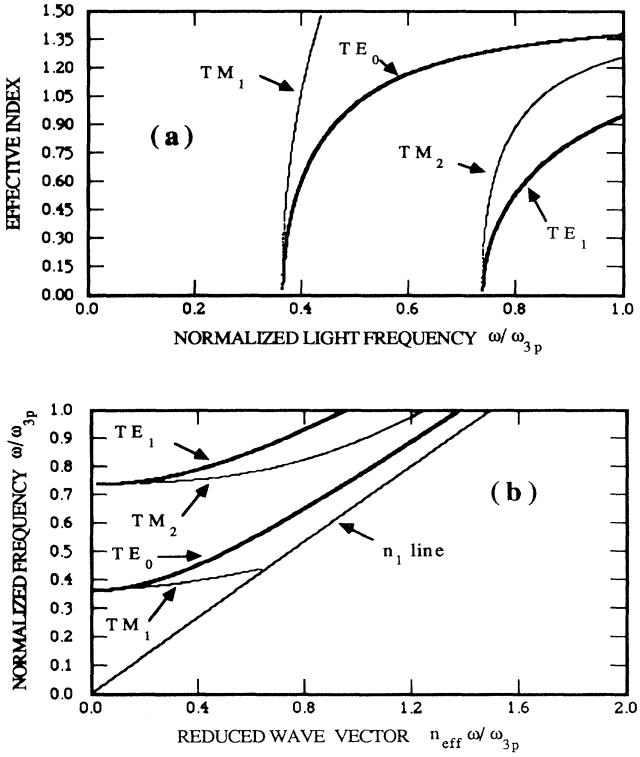

FIG. 38. (a) Frequency dispersion of the effective index of TE and TM oscillating guided modes vs ω/ω_{3p} for the following parameters: $n_1=1.5$, $q=2$, $\tau=0.8$. For a metal such as gold with $\lambda_{3p}=460$ nm, the corresponding thickness is $a=150$ nm. (b) Frequency dispersion of TE and TM oscillating guided modes. ω-β representation. The following values of the parameters have been adopted: $n_1=1.5$, $q=2$, $\tau=0.8$.

Examples of the frequency dispersion curves for the effective index are shown in Figs. 38(a) and 38(b).

CONCLUSION

A complete discussion of guided optical modes in planar heterostructures consisting either of a normal dielectric sandwiched between two media with negative dielectric constants or a medium with a negative dielectric constant surrounded by two normal dielectrics has been presented. All media have been assumed to be lossless and a plasma frequency dispersion law has been taken for the media with negative dielectric constants.

In the first case, transverse magnetic modes with field amplitude maxima at the interfaces (surface modes) are found as stable mathematical solutions. The set of solutions and their cutoffs depend sensitively on the inner layer thickness (geometric dispersion) and the light frequency. Examples pertaining to realistic cases have been presented. The well-known Fano modes are recovered as special solutions in the symmetric cases.

In the second case, both TM surface modes and TM and TE oscillating guided modes are found as stable, unattenuated solutions. Again the geometric and frequency dispersion is discussed in the general case. Particular examples have been presented for realistic cases.

It would also be interesting to examine other types of simple topological situations, such as the circular cylindrical case (optical fibers surrounded by a metallic layer). They will be treated in a forthcoming paper.

ACKNOWLEDGMENTS

The Laboratoire d'Optique Appliquée is "Unité Associée au Centre National de la Recherche Scientifique No. 1406."

---

*Also at Groupe de Physique des Solides, Université Paris, VII, France.

[1]D. Marcuse, *Theory of Dielectric Waveguides* (Academic, New York, 1974).

[2]A. Snyder and J. D. Love, *Optical Waveguide Theory* (Chapman and Hall, New York, 1983).

[3]*Surface Polaritons; Electromagnetic Waves at Surfaces and Interfaces,* edited by W. M. Agranovich and D. L. Mills (North-Holland, Amsterdam, 1982).

[4]*Electromagnetic Surface Waves,* edited by A. D. Boardman (Wiley, New York, 1982).

[5]H. Raether, in *Surface Plasmons on Smooth and Rough Surfaces and on Gratings* (Springer-Verlag, Berlin, 1988); *Physics on Thin Films,* edited by G. Hass, M. H. Francombe, and R. W. Hoffmann (Academic, New York, 1977), Vol. 9, p. 145.

[6]H. G. Unger, *Planar Optical Waveguides and Fibres* (Clarendon, Oxford, 1980).

[7]B. Prade and J. Y. Vinet, *Optique Guidée, Première Partie: Théorie de Quelques Guides Simples* (ENSTA, Paris, 1987).

[8]L. Landau and E. Lifchitz, *Electrodynamics of Continuous Media* (Pergamon, New York, 1960), Chap. 64.

[9]J. J. Burke, G. I. Stegeman, and T. Tamir, Phys. Rev. B **33**, 5186 (1986), and references cited therein.